Quantitative evaluation of the dynamics of proton transfer from photoactivated bacteriorhodopsin to the bulk

E. Nachliel*, M. Gutman

Laser Laboratory for Fast Reactions in Biology, Department of Biochemistry, Tel Aviv University, Ramat Aviv 69978, Israel

Received 11 June 1996; revised version received 16 July 1996

Abstract **It has been reported by many research groups that protons released during the photocycle of bacteriorhodopsin are detected by surface bound indicators much faster than by indicators in the bulk. In this study we used numerical simulation of chemical reaction's dynamics for analyzing the delayed appearance of protons in the bulk. The results indicate that the low p*K* surface groups of the membrane, which form an undilutable concentrated matrix of proton binding sites, retain the protons in this space according to the mass action law. The main sites for proton accumulation are the cluster of carboxylates on the cytoplasmic side of the membrane. The protonation of an indicator in the bulk does not proceed by its reaction with free proton, but rather through self-diffusion of the indicator to the membrane and abstraction of proton from the protonated surface group. The detailed mechanisms which correspond with these reactions are reported.**

Key words: Dynamics; Proton transfer; Photoactivated bacteriorhodopsin

1. Introduction

Bacteriorhodopsin carries out a complex sequence of intraprotein reactions which convert the delta function perturbation of an absorbed photon into an envelope of reversible proton transfer reactions stretching over few milliseconds. The protons are released by the protein on the extracellular (EC) side of the membrane and taken up later at the cytoplasmic (CP) face [1]. The sequence of release and uptake can be modulated either by the external pH, or by mutation of the intrachannel acceptor elements located on the EC channel of the protein [1,2].

For a long time interest was focused on the intraprotein machinery that drives the spatially unidirectional proton transfer. Since the beginning of this decade attention has also been paid to the mechanism of proton transfer from the protein to the bulk.

The experimental system, first introduced by Heberle and co-workers [3–5], is based on selective labeling of the protein (or of a lipid in the membrane) by fluorescein (Flu) and measuring the dynamics of its protonation following a pulse irradiation. All these measurements recorded the protonation of the protein bound dye within the same time window of the appearance of the M state. It was also noticed that an indicator bound to the cytoplasmic side of the purple membrane (PM) is protonated within the same time frame [6–8], namely the passage of the proton from the EC to the CP side is very fast. Yet, as calculated by Heberle et al. [5], the diffusion coefficient estimated from the time constants of the reaction is smaller than the diffusion coefficient of proton in bulk water (3.4×10^{-7} vs. 9.3×10^{-5} cm^2/s, respectively). While these observations are compatible with standard biophysical formalism, a surprising result was recorded when the protons were detected by an indicator that resides in the bulk. Pyranine (8-hydroxypyrene-1,3,6-trisulfonate) (ϕOH) does not adsorb to negatively charged purple membranes [9,10], thus its protonation measures how fast the acidic pulse propagates to the bulk. The rate of this reaction was measured by many research groups [3–8]. In all cases it was found that the protonation of the pyranine was delayed by a few hundred microseconds behind the protonation of the fluorescein. There appears to be no obvious mechanism that accounts for the measured delay.

The fact that an indicator in the bulk follows dynamics that differ from that on the surface implies that the evaluation of the observation must rely on a detailed kinetic analysis, which accounts for the effect of sessile buffer moieties on the diffusion of protons [11,12]. In previous publications, comparison between the protonation of the bulk indicator, surface indicator and the M state was based on descriptive formalism. The observed time envelope of the measured species (M, FluH or ϕOH) was presented as a sum of exponents. This kind of quantitation is very convenient for comparative, intuitive presentation. Yet, it should be remembered that time constants of a multistep reaction are not directly related to the first order or second order rate constants which are the only parameters that can be quantitatively interpreted.

The first quantitation of the rate constants for proton association with the surface of bacteriorhodopsin preparation was carried out in our laboratory [13,14]. In these studies we used the photo-inactive bacterio-opsin membrane, labeled by fluorescein at K 129 (EC), or on the CP side when bound to the D36C or D38C mutated proteins. The samples were acidified by photo-excitation of the pyranine, and excited state proton emitter [15] present in the bulk. Detailed analysis of the reversible proton exchange between the dye in the bulk and that on the membrane yielded the first and the second order rate constants of the acid-base interactions. The experiments were then repeated with the photoactive BR preparations. The measured rate constants were comparable to those measured with the bacterial-opsin.

Based on these studies it was concluded that the major pathway for the propagation of the acidic perturbation and its subsequent relaxation to the initial state proceeds by collisional proton transfer between mobile and sessile proton bind-

*Corresponding author.

Abbreviations: BR, bacteriorhodopsin; Flu, FluH, ionized and protonated states of fluorescein; ϕO^-, ϕOH, ionized and protonated states of 8-hydroxypyrene-1,3,6-trisulfonate; COO^-_{CP}, COO^-_{EC}, the carboxylic groups on the cytoplasmic and extracellular face of the membrane, respectively.

PII S0014-5793(96)00870-8

ing sites. Within less than 1 μs after the excitation pulse all free protons are adsorbed by the various buffering sites and their state of protonation (BH/B^-) is offset with respect to their equilibrium ratio (see Fig. 1). The relaxation of the system back to the state of equilibrium proceeds by collisional proton transfer. The pyranine anion is reprotonated not by reacting with free proton in the bulk; it diffuses to the membrane to abstract a proton from carboxylate (or Flu H) on the PM surface. The rate constants of these reactions were determined within ± 5% of accuracy [13,14].

The exchange of protons by the surface group behaves as a virtual collisional proton transfer. The high density of the proton binding moieties on the surface (less than 100 $Å^2$ per site accounting for the anionic lipids) generates a situation where the surface consists of an undilutable concentrated solution of protonable moieties (equivalent to a solution of ~ 1 M). Thus, a proton released from a site within this matrix will have a greater probability of reacting with the next site rather than with a molecule in the bulk. This perpetual, release and binding sequence is the major cause of proton delay on the surface. The discharge of proton to the bulk is controlled by the density of the protonable sites on the surface and the concentration of the diffusing proton binding molecules (pyranine or buffer) [16,17]. This mechanism has been experimentally and theoretically investigated by Gutman, Nachliel and co-workers [12,18–20].

In the present communication it is our wish to implement this quantitative mode of analysis for evaluation of the observed dynamics of the photocycle driven protons with surface indicators bound to BR and with pyranine as pH indicator in the bulk.

As will be shown below, the delay of protons at the surface of the protein is accountable by the high buffer capacity of the membrane.

2. Materials and methods

The differential rate equations used for the simulation of the dynamics and the program that solves them were written in our laboratory and are available upon request.

The experimental tracings were measured by L.S. Brown and J.K. Lanyi (Biochemistry and Physiology, UC, Irvine, CA). The experiments were carried out with the V130C mutated BR preparation imbedded in polyacrylamide and equilibrated with 100 mM NaCl. The protein concentration was 16 μM. The fluorescein was linked by iodoacetamide to the cyts at 130 with ~100% yield. The pyranine concentration, when present, was 50 μM. The pH of the measurements was 7.0 and 6.9 for the fluorescein-labeled protein and unlabeled protein in the presence of pyranine, respectively. The fluorescein signals were duly corrected for the spectral contribution of the protein. The pyranine signal was corrected by subtracting the absorbance changes as measured in the presence of 20 mM buffer (for more details see [21]).

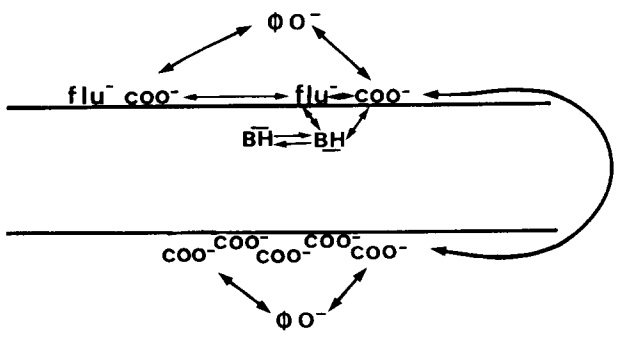

Scheme 1.

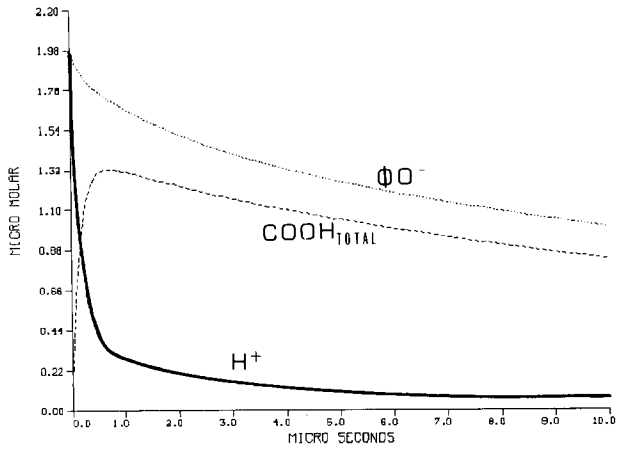

Fig. 1. Dynamic reconstruction of the reactions following a pulse acidification of PM preparation by photo-excited pyranine. The curves are the numerical reconstruction of the experiments detailed in [13]. 11.9 μM bacteriorhodopsin membranes, labeled by fluorescein at K129, were suspended in a 25 μM solution of pyranine (pH 7.3) and excited by a laser pulse. At zero time 1.98 μM of H^+ and pyranine anion were formed in the bulk. The free proton concentration (———) decays rapidly and within 500 ns ~80% were taken up by the carboxylates of the membrane (- - -). The rate of protons uptake by the pyranine anion (· · ·) is rather slow, demonstrating the high capacity of the surface carboxylate to compete for the protons. The incremental proton concentration, 10 μs after the pulse, has a negligible contribution to the relaxation of the perturbation.

In accord with the data published by other groups [3–8], the measurements with pyranine were carried out with unlabeled protein and the fluorescein-labeled preparations were measured in the absence of pyranine.

The simulation of the curves was carried out in tandem both for the M state formation and the indicator (either fluorescein or pyranine). All rate constants which had been determined before [13,14] were used without any modification. The pK of the pyranine and the carboxylate on the EC face and the cluster of 5 carboxylates on the CP side were taken as determined previously [13,14]. The pK of the fluorescein on C130 was measured by titration.

3. Results and discussion

3.1. Intraprotein dynamics

The ultrashort event of photon absorption by retinal drives a sequence of reactions leading to complex evolution of the M intermediate and release of protons. In the present study we concentrated only on the proton discharge phase of the photocyle while the events linked with the reprotonation of the protein were omitted. Accordingly our simulation corresponds with the first 1 ms of the dynamics.

The conversion of the delta function perturbation into the complex dynamics of the M intermediate was done by adherence to the known mechanism of the photocycle, subjected to minor simplifications. The perturbation in our model is the formation of the L state, generated at $t = 0$, in a quantity equal to the concentration of M as measured at the maximum of its curve. The L state decays by transferring a proton to a cluster identified with the residues of D85, D212 and R82. This cluster, upon protonation, interacts with a surface group identified by Lanyi and co-workers [22] as E204, shifting it from a high pK state (BH, pK = 9.3) [23] to a low one (<u>BH</u>, pK = 5.8)

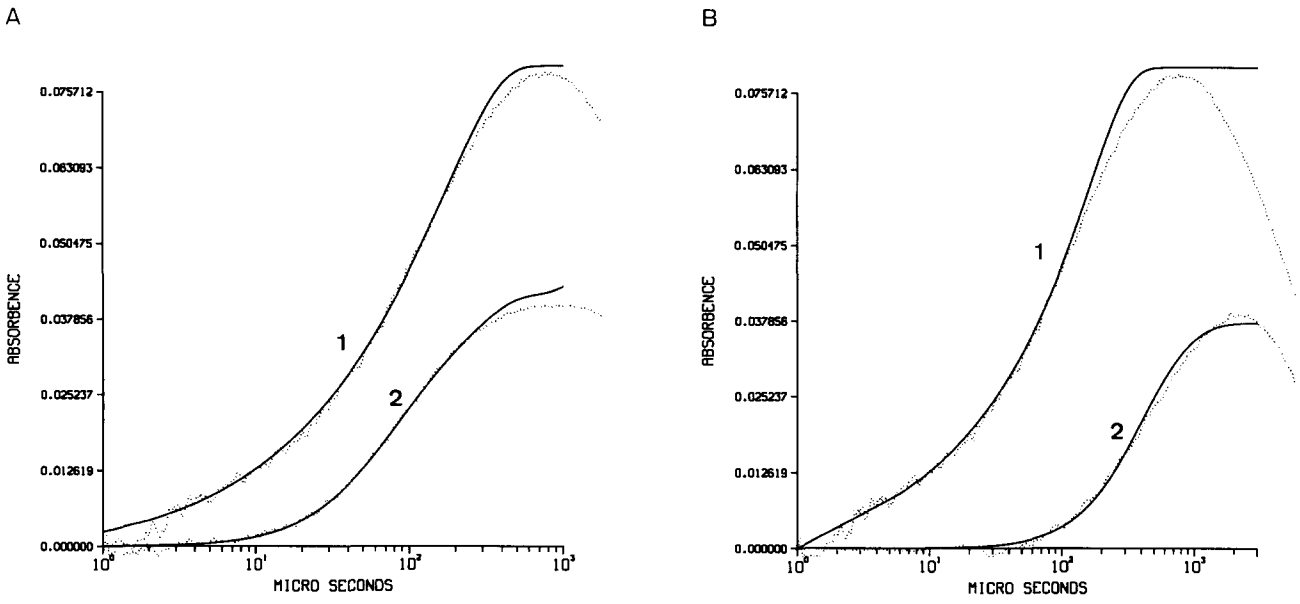

Fig. 2. Dynamic reconstruction of protein-bulk proton transfer between photoactivated PM and pyranine in the bulk. The experimental tracings, measured as detailed in [22], were fitted by numeric simulation as described in the text. (A) Curve 1 corresponds with the formation of the deprotonated Schiff base. The experimental parameter was the M state, recorded at 412 nm, while the fitted curve is $(L_{(0)}-L_{(t)})$, where $L_{(0)}$ is the initial perturbation and $L_{(t)}$ is the amount of L at time t. Curve 2 is the protonation of the fluorescein covalently attached to cysteine replacing V130. The theoretical curve was calculated using the rate constants given in Table 1. (B) Curve 1 corresponds with the evolution of the M state as in (A). Curve 2 simulates the protonation of pyranine (50 μM) added to the bulk.

[23,24]. This two-step mechanism, with its appropriate rate constants, suffices to reconstruct the dynamics of M formation given by the expression $M_{(t)}=L_{(0)}-L_{(t)}$ and to generate an acidic group at the surface of the protein.

The purpose of these reactions was solely to generate the M dynamics coupled with the formation of low pK group BH. For this reason the rate constants of these steps have no physical meaning and are not to be interpreted.

3.2. Dispersion of the acidic pulse to the bulk

The mechanism of proton dispersion to the surface and bulk is given in {{Scheme 1. The BH moiety is at equilibrium with all protonable groups in the system yet being the strongest base, it is initially in its full protonated state. Once the system is perturbed (equivalent to the formation of L at the quantity $L_{(0)}$), the BH is gradually shifted to the low pK state BH. The low pK state BH interacts by reversible proton transfer with the single reactive carboxylate present on the EC side of the protein [13,14] and with the fluorescein (at K130C) if present in the preparation.

Protons released on the surface of the photoactivated BR molecules disperse all over the purple membrane. The initially protonated carboxylates and the fluorescein moieties transfer their protons to the other protonable moieties on the surface. The distribution of protons was quantitated by a virtual second order rate constants that comply with the free energy relationship. The ratio between the forward and the backward rate constants is proportional with the ΔpK between the reactants. We accounted in our simulation for proton transfer from the moieties on the photoactivated protein (2.2 μM) with the rest of the protein population (13.8 μM) (see Table 1). The same formalism was used to equate for proton transfer between the two sides of the membrane. All these reactions are described by virtual second order rate constants whose magnitude can be used only for comparative purposes [19,20]. On the other hand, the protonation of the pyranine is a true second order diffusion controlled reaction [13,14] which was determined within 5% accuracy. The linkup of the two systems into an integrated one was achieved by using the same virtual rate constants common to both systems when reconstructing the dynamics of each of them. Thus by this conjuncture we linked the two sets of experiments, where the fluorescein or the pyranine are monitored in tandem with M, into a single analyzable system with fewer degrees of freedom.

The simulation of the experimental curves by the numeric integration implies that the same set of seven differential rate equations had been solved for 200 time points. At each time point the discrete value of two pairs of vectors $M_{(t)}$ plus Flu $H_{(t)}$ and $M_{(t)}$ plus $\phi OH_{(t)}$ were calculated to fall within the noise envelope of the experimental result. Considering the fact that the time span varied by 3 orders of magnitude (1 μs–1 ms) and the concentrations of the measured vectors varied by 2.5 orders of magnitude, we regard such a solution as sufficiently redundant to take the adjustable parameters as true representatives of the system.

The simulated dynamics of $M_{(t)}$, Flu $H_{(t)}$ and $\phi OH_{(t)}$ are shown in Fig. 2. The fit, with respect to the measured vector, is very good, up to the point where the reprotonation of the BR reverses the course of the reaction.

The parameters used for reproducing the curves are given in Table 1.

3.3. The mechanism of proton dispersion at the molecular level

The dispersion of protons following the L formation among the various groups is given in Figs. 3 and 4. These figures depict, in molar units, the protonation transients of the participating groups.

Fig. 3 describes the dynamics where the protons are detected by the bulk indicator – the pyranine. Five lines are drawn in this figure. The uppermost one corresponds with

the M state formation (curve 1). Following the perturbation, the BH species (curve 2) appears very rapidly, with the same onset of the M state. Yet, due to its low pK, it loses its proton and fades while the other protonated products are accumulating (curves 3–5). The protons lost by BH are initially taken up by the EC carboxylate (curve 3). The dwell time of a proton on a carboxylic acid having a pK = 4.85 is ~3 μs [19,20], thus no appreciable accumulation of $COOH_{EC}$ takes place. The dispersion of protons over the purple membrane is facilitated by its low pK moieties (phospholipid and sulfo-lipid, about 10 acidic sites per BR). The spatial density of these sites is comparable to that of a 1 M solution. A proton discharged from a carboxylate can react with these sites, temporarily replacing the native counterion, redissociate and react with other temporary binding sites. Controlled experiments carried out by Nachliel and Gutman [18] had demonstrated that a low pK moiety (pK = 2.25), such as the phospho anion of phosphatidylcholine, acts as a better proton relay element than a less acidic one like phosphatidylserine (pK = 4.6). Thus, the low pK phospho and sulfo lipids assist in the rapid spreading of the proton. The involvement of the multiple 'bind and release' mechanism is also evident by the lower apparent diffusion coefficient of protons at the PM surface [5]. The protons tend to accumulate on the carboxylates of the cytoplasmic face (curve 4) of the membrane. These carboxylates (pK = 5.15) appear as a cluster of 5 carboxylates [13,14] which are so close that their Coulomb cages merge into a single, highly efficient proton trap. The rate of the reaction of that cluster with free protons is comparable to the protonation of the pyranine anion (3×10^{10} M^{-1} s^{-1} vs. 5×10^{10} M^{-1} s^{-1}, respectively). The proximity between these carboxylates, together with their capacity to exchange proton among them, endorse this cluster with a competitive edge with respect to the pyranine anion and its protonation precedes that of pyranine. Only after an appreciable time (~200 μs), the higher basicity of the pyranine (pK = 7.7 vs. 5.15) tips the balance and the protonation of the pyranine is at the expense of the cytoplasmic carboxylates (curve 5). Comparison of the second order rate constant of protonation of the soluble pyranine by the surface carboxylates (two bottom lines, Table 1) reveals that the reaction with the negatively charged CP face is ~100 times slower than the reaction with the EC one. Yet, due to the fact that the protons concentrate on the CP face, their dispersion to the bulk is slow and the rise of ϕOH (curve 5) is delayed in time and coincides with the deprotonation of the CP carboxylates.

Table 1
Rate constants of proton exchange reactions on the surface of purple membranes

Reaction	Rate constants (M^{-1} s^{-1})
BH[a]+Flu^- *	$2.5\pm0.1\times10^{10}$
BH+COO^-_{EC}* [b]	$5.0\pm0.5\times10^{10}$
FluH *+Flu^-[c]	$4.5\pm0.5\times10^{7}$
$COOH_{EC}$ *+Flu^-	$5.0\pm0.5\times10^{9}$
$COOH_{EC}$+COO^-_{CP}[d]	$0.8\pm0.2\times10^{9}$
ϕO^-[e]+$COOH_{EC}$	$5.0+2.0\times10^{9}$
ϕO^-+$COOH_{CP}$	1.0×10^{7}

*Compounds on the surface of the photocycled protein's molecules.
[a]BH is the low pK state of the proton releasing group, pK = 5.8. The high pK state BH has a value of 9.3.
[b]The extracellular carboxylate pK = 4.85 ± 0.05.
[c]The fluorescein attached to Cys-130. pK = 7.55.
[d]The cytoplasmic carboxylate cluster pK = 5.15 ± 0.1.
[e]The pyranine anion in the bulk. pK = 7.7.

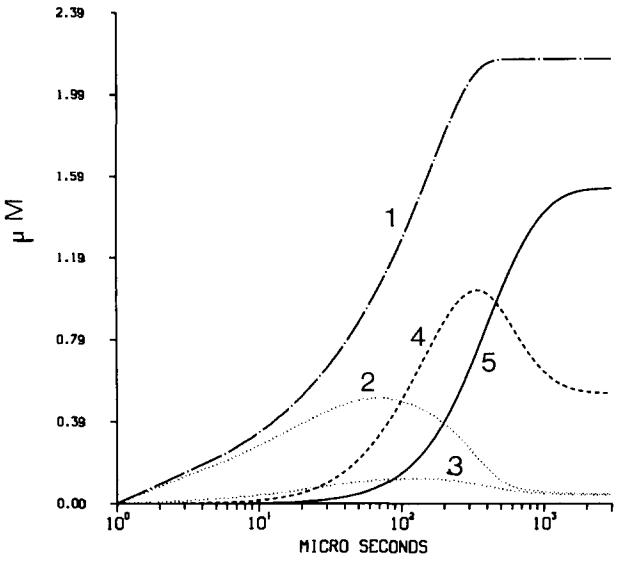

Fig. 3. Detailed mechanism of proton transfer between photoactivated purple membrane and pyranine in the bulk. The curves simulate the result shown in Fig. 1B and are given in molar units. Curve 1 is the one reproducing the M state in Fig. 1B. Curve 2 shows the appearance of the low pK state of BH which fades to the transfer of its proton to COO^-_{EC} (curve 3) and COO^-_{CP} (curve 4) and to pyranine (curve 5).

Fig. 4 depicts the scenario in the absence of a soluble proton acceptor or any bulk buffer while the fluorescein, on the EC surface, functions as the highest pK proton acceptor of the system (pK = 7.55). Curve 1 is the formation of the M intermediate, curve 2 depicts the evolution of the protonated state of the fluorescein while curves 3 and 4 are of the protonated state of the EC and CP carboxylates. The dynamics of BH (not shown) is practically similar to that drawn in Fig. 3, curve 2, but the dynamics of the $COOH_{EC}$ is altered. Its envelope is shallower due to proton loss to the nearby fluorescein. The protons discharged from the low pK state of BH are distributed between the carboxylate of the EC side and the fluorescein. These carboxylates, via the low pK conduit system made of the acidic lipids [18], spread the protons over the whole surface and the cytoplasmic cluster is once again an efficient competitor with respect to the fluorescein of the extracellular face. In this figure we drew in the inset the total protonation of fluorescein ($FluH_{tot}$) together with the breakdown of the dynamics for the protonation of the fluorescein molecule present on photon-activated protein and those present on the non-cycled BR molecules. The first fluorescein molecules which are protonated are those bound to the photoactivated BR proteins (13% of the total content). Their protonation is fast and their contribution to the signal is about half of the measured transients. The rest of the fluorescein signal is generated after a time delay, comparable to that of the protonation of the pyranine in the bulk (compare with curve 5 in Fig. 3). The breakdown of the fluorescein protonation to a sum of two parallel reactions explains its reported multiphasic dynamics [3–8].

In this study we combined the precise chemical kinetics, based on time-resolved measurements of bulk-surface proton transfer, with the empirical measurements of proton discharge

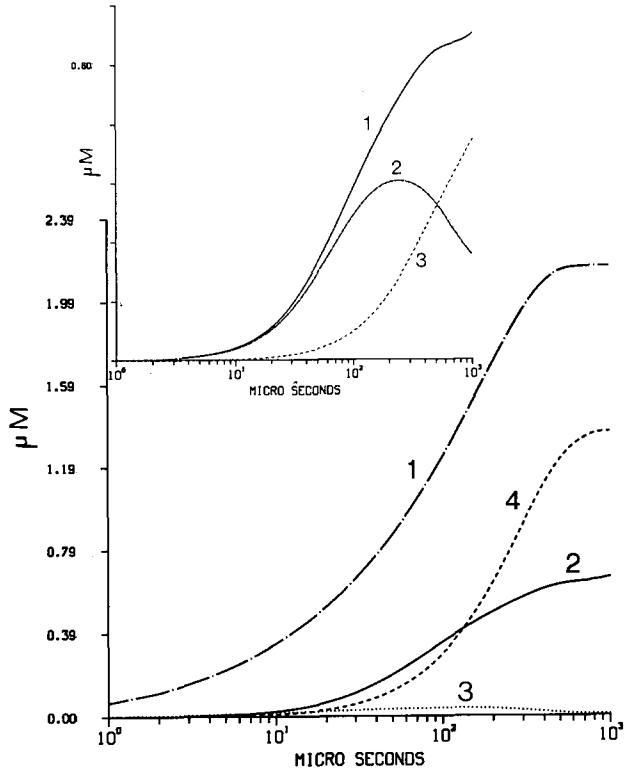

Fig. 4. Detailed mechanism of proton transfer between photoactivated purple membrane preparation and its surface groups. The curves simulate the results shown in Fig. 1A and are given in molar units. Curve 1 corresponds with the formation of the M state. Curve 2 reconstructs the protonation of the fluorescein attached to Cys-130. Curve 3 depicts the reversible protonation of the EC carboxylate and curve 4 is for the CP carboxylates cluster. Inset: detailed dynamics of the protonation of fluorescein. Curve 1 corresponds with the observed protonation signal, as shown in the main frame. Curve 2 is the protonation of fluorescein molecules attached on the photocycling BR molecules while curve 3 depicts the protonation of fluorescein bound to the non cycling protein molecules.

from photoactivated bacteriorhodopsin. As shown above there is no contradiction between the two. The delayed appearance of proton in the bulk is quantitatively reconstructed by the rigorous analysis. The source of the delay is attributed to the high density of ionizable groups on the surface. The low pK ones tend to exchange proton among themselves while the cytoplasmic carboxylates cluster, with the higher pK groups, acts as a temporal delay system.

We have clearly demonstrated that the dynamics of protonation is controlled by two independent terms: the first is the dynamic competition for protons, which favors the protonation of moieties which are close to each other. The second is the thermodynamic advantage of the higher pK moiety that can collect protons from the surrounding low pK groups. It is the combination of the two processes which controls the apparent dynamics as measured in multicomponent, multistep processes such as the photocycle. It must be explicitly stated that the delay of proton release to the bulk is not due to a 'thermodynamic barrier which prevents the free proton movement from the surface to the bulk' [25]. The delay is a direct consequence of the dwell time of protons on the proton binding sites of the surface which affects both the dynamics of surface groups (see inset to Fig. 4) and the bulk phase indicator in the same way.

Finally, we wish to point out that the carboxylate cluster of the cytoplasmic surface is kinetically competent to act as the main proton binding site of the CP side of the BR. This site may be the one which effectively abstracts a proton from the well buffered neutral interior of the cell and funnels it to the photodriven machinery that pumps it out. Similar functioning carboxylates have also been detected on the N side of the mitochondrial membrane [24].

Acknowledgements: This research is supported by a grant from the Israel Science Foundation (538/95). The authors are grateful to L.S. Brown and J.K. Lanyi for sharing their experimental results with us.

References

[1] Lanyi, J.K. (1993) Biochim. Biophys. Acta 1183, 241–261.
[2] Brown, L.S., Yamazaki, Y., Maeda, A., Sun, L., Needleman, R. and Lanyi, J.K. (1994) J. Mol. Biol. 239, 401–414.
[3] Heberle, J. and Dencher, N.A. (1990) FEBS Lett. 277, 277–280.
[4] Heberle, J. and Dencher, N.A. (1992) Proc. Natl. Acad. Sci. USA 89, 5996–6000.
[5] Heberle, J., Riesle, J., Thiedenmann, G., Osterhelt, D. and Dencher, N.A. (1994) Nature 370, 379–382.
[6] Scherrer, P., Alexiev, U., Marti, T., Khorana, H.G. and Heyen, M.P. (1994) Biochemistry 33, 13684–13692.
[7] Alexiev, U., Marti, T., Heyen, M.P., Khorana, H.G. and Scherrer, P. (1994) Biochemistry 33, 13693–13699.
[8] Alexiev, U., Mollaaghababa, R., Scherrer, P., Khorana, H.G. and Heyen, M.P. (1995) Proc. Natl. Acad. Sci. USA 92, 372–376.
[9] Jonas, R., Koutalos, Y. and Ebrey, T.G. (1990) Photochem. Photobiol. 52, 1163–1177.
[10] Kates, M., Kushwaha, S.C. and Sprott, G.D. (1982) Methods Enzymol. 88, 98–111.
[11] Junge, W. and McLaughlin, S. (1987) Biochim. Biophys. Acta 890, 1–5.
[12] Gutman, M. and Nachliel, E. (1990) Biochem. Biophys. Acta 1015, 391–414.
[13] Nachliel, E., Gutman, M., Kiryati, S. and Dencher, N.A. (1996) Proc. Natl. Acad. Sci. USA, in press.
[14] Yaniv-Checover, S. (1996) M.Sc. Thesis.
[15] Gutman, M. (1986) Methods Enzymol. 127, 522–538.
[16] Drachev, L.A., Kaulen, A.D. and Skulachev, V.P. (1984) FEBS Lett. 178, 331–335.
[17] Grzesiek, S. and Dencher, A.N. (1986) FEBS Lett. 208, 337–342.
[18] Nachliel, E. and Gutman, M. (1988) J. Am. Chem. Soc. 110, 2629–2635.
[19] Gutman, M., Nachliel, E. and Tsfadia, Y. (1995) in: Permeability and Stability of Lipid Bilayers (Disalvo, G.A. and Simons, S. eds.) pp. 259–276, CRC Press, Boca Raton, FL.
[20] Gutman, M. and Nachliel, E. (1995) Biochim. Biophys. Acta 1231, 123–138.
[21] Cao, Y., Brown, L.S., Saski, J., Maeda, A., Needleman, R. and Lanyi, R.J. (1995) Biophys. J. 68, 1518–1530.
[22] Brown, L.S., Sasaki, J., Kandori, H., Maeda, A., Needleman, R. and Lanyi, K.J. (1995) J. Biol. Chem. 270, 27122–27126.
[23] Kono, M., Misra, S. and Ebrey, T.G. (1993) FEBS Lett. 331, 31–34.
[24] Cao, Y., Brown, L.S., Needleman, R. and Lanyi, J.K. (1993) Biochemistry 32, 10239–10248.
[25] Teissie, J. (1996) Nature 379, 305–306.